PHYSICAL REVIEW D **75,** 083526 (2007)

Precise constraints on the dark matter content of Milky Way dwarf galaxies for gamma-ray experiments

Louis E. Strigari,[1,*] Savvas M. Koushiappas,[2,†] James S. Bullock,[1,‡] and Manoj Kaplinghat[1,§]
[1]*Center for Cosmology, Department of Physics and Astronomy, University of California, Irvine, California 92697, USA*
[2]*Theoretical Division and ISR Division, MS B227, Los Alamos National Laboratory, Los Alamos, New Mexico 87545, USA*
(Received 7 December 2006; published 30 April 2007)

We examine the prospects for detecting γ-rays from dark matter annihilation in the six most promising dwarf spheroidal (dSph) satellite galaxies of the Milky Way. We use recently measured velocity dispersion profiles to provide a systematic investigation of the dark matter mass distribution of each galaxy, and show that the uncertainty in the γ-ray flux from mass modeling is less than a factor of ~ 5 for each dSph if we assume a smooth Navarro-Frenk-White (NFW) profile. We show that Ursa Minor and Draco are the most promising dSphs for γ-ray detection with GLAST and other planned observatories. For each dSph, we investigate the flux enhancement resulting from halo substructure, and show that the enhancement factor relative to a smooth halo flux cannot be greater than about 100. This enhancement depends very weakly on the lower mass cutoff scale of the substructure mass function. While the amplitude of the expected flux from each dSph depends sensitively on the dark matter model, we show that the flux ratios between the six Sphs are known to within a factor of about 10. The flux ratios are also relatively insensitive to the current theoretical range of cold dark matter halo central slopes and substructure fractions.

DOI: 10.1103/PhysRevD.75.083526 PACS numbers: 95.35.+d, 14.80.Ly, 98.35.Gi, 98.62.Gq

I. INTRODUCTION

In the ΛCDM cosmological model, cold dark matter (CDM) comprises approximately one-fourth of the total energy density of the Universe [1]. However, the nature of dark matter remains unknown. Extensions to the standard model, such as those based on supersymmetry [2,3] and universal extra dimensions [4], predict the existence of stable, weakly interacting massive particles (WIMPs) with mass $\sim[10^1–10^4]$ GeV, which provide excellent candidates for cold dark matter. In these models, WIMPs interact gravitationally as well as weakly, therefore WIMP annihilation can produce γ-ray photons.

Present and next-generation γ-ray observatories such as STACEE [5], HESS [6], MAGIC [7], VERITAS [8], CANGAROO [9], GLAST [10], and HAWC [11] will search for the signatures of dark matter annihilation. The nearest location to search for this signal is the center of the Milky Way, although uncertain backgrounds from astrophysical sources would make the clean extraction of such a signal difficult [12–14]. Additionally, there is wide empirical uncertainty as to the shape of the central dark matter density profile, which may have been altered by the growth of a supermassive black hole [15,16] or any process which can exchange energy between the baryonic and dark matter components (e.g. [17–19]).

In the case of dwarf spheroidal galaxies (dSphs), astrophysical backgrounds and baryonic-dark matter interactions are expected to be largely absent. The Milky Way system contains at least 18 dSphs, which are observed to be low-luminosity systems with an extent $\sim$kpc. Based on their stellar mass-to-light ratios, dSphs contain of order $\mathcal{O}(10^1–10^2)$ more mass in dark matter than in visible light [20] and thus are ideal laboratories for studies that are sensitive to the distribution of dark matter. Furthermore, their relative proximity and high galactic longitude and latitude makes them ideal for high signal-to-noise detection.

In this paper, we consider the prospects for γ-ray detection from dark matter annihilation in six dSphs of the local group. The six dSphs are selected because of both their proximity and estimated masses, the latter of which is based on the most recent measurements of their velocity dispersion profiles. We estimate the range of allowable distributions of dark matter that satisfy the observed velocity dispersion profiles, and deduce the γ-ray flux expected from each dSph. We focus on quantifying the uncertainty in the predicted fluxes that comes from the dark matter density distribution in each system. As part of this uncertainty, we determine the flux contribution of substructure within the dSph dark matter halos.

Past work in the literature considered detecting γ-rays from dark matter annihilation in Milky Way-bound dark matter halos: dSphs were studied in [14,21–24], more massive galaxies in the local group were considered in [25], potentially dark subhalos were studied in [26–31], and the prospects of detecting microhalos were explored in [32,33].

In comparison to previous studies of dSphs, our work is the first to combine theoretical predictions for CDM halo profile shapes and normalizations with specific dynamical constraints for each observed system. Though the observed velocity dispersion profiles are equally well fit by both

---

[*] Electronic address: lstrigar@uci.edu
[†] Electronic address: smkoush@lanl.gov
[‡] Electronic address: bullock@uci.edu
[§] Electronic address: mkapling@uci.edu

central density cores and cusps, we restrict ourselves to inner profile shapes $\rho \propto r^{-\gamma}$ with $\gamma \simeq 0.7$–1.2 [34,35], because this is what is expected for the subset of dark matter candidates that actually annihilate into photons (CDM). We show that the primary uncertainty in the smooth dark matter flux contribution for CDM halos comes not from the relatively narrow range of central cusp slopes, but from the density and radius *normalization* parameters, ρ_s and r_s for the halo. As we show below, the published velocity dispersion data along with the predicted relations between ρ_s and r_s for CDM halos allow a tight constraint on the dark-halo density contribution to the annihilation signal.

While the value of the expected flux signal for each dSph is sensitive to the (unknown) nature of the underlying dark matter candidate, we demonstrate that the *relative* flux from system to system is significantly constrained. Ursa Minor is the most promising dSph candidate for detection and we present the expected γ-ray flux ratios between the remaining five dSphs and Ursa Minor. We also demonstrate that enhancement of the signal due to the presence of substructure in dSph halos themselves increases the predicted fluxes by at most a factor of ~ 100.

This paper is organized as follows. In Sec. II, we discuss the γ-ray annihilation signal expected from CDM halos and the enhancement of the flux due to the presence of substructure within the dSph dark matter halos. In Sec. III we discuss the dynamical modeling of the dSph galaxies. In Sec. IV we present our results, and we conclude in Sec. V. Throughout the paper, we assume a ΛCDM cosmological model with $\Omega_{\rm m} = 0.3$, $\Omega_\Lambda = 0.7$, $h = 0.7$, and $\sigma_8 = 0.9$.

II. GAMMA-RAYS FROM ANNIHILATION IN COLD DARK MATTER HALOS

The γ-ray flux from dark matter annihilation in a dark matter halo with characteristic density ρ_s and radius r_s at a distance $\mathcal{D}$ may be written as

$$\frac{dN_\gamma}{dAdt} = \frac{1}{4\pi}\mathcal{P}[\langle\sigma v\rangle, M_\chi, dN_\gamma/dE]\mathcal{L}(\rho_s, r_s, \mathcal{D}). \tag{1}$$

We have explicitly divided the flux into a term that depends only on the dark matter particle and its annihilation characteristics, $\mathcal{P}(\langle\sigma v\rangle, M_\chi, dN_\gamma/dE)$, and one that depends only on the density structure of the dark matter halo, the distance to the halo, $\mathcal{D}$, and the angular size over which the system is observed, $\mathcal{L}(\rho_s, r_s, \mathcal{D})$. The structure quantity $\mathcal{L}$ is defined as

$$\mathcal{L} = \int_0^{\Delta\Omega}\left\{\int_{\rm LOS}\rho^2[r(\theta, \mathcal{D}, s)]ds\right\}d\Omega, \tag{2}$$

where the integral is performed along the line of sight over a solid angle $\Delta\Omega = 2\pi(1-\cos\theta)$. The term that contains the microscopic dark matter physics is given explicitly as

$$\mathcal{P} = \int_{E_{\rm th}}^{M_\chi}\sum_i \frac{dN_{\gamma,i}}{dE}\frac{\langle\sigma v\rangle_i}{M_\chi^2}dE. \tag{3}$$

Here, the mass of the dark matter particle is M_χ, the annihilation cross section to a final state "i" is $\langle\sigma v\rangle_i$, and the spectrum of photons emitted from dark matter annihilation to that final state is $dN_{\gamma,i}/dE$. Our goal is to use observed velocity dispersion profiles to empirically constrain the $\mathcal{L}$ term. This allows observations from γ-ray telescopes to more effectively constrain the particle nature of dark matter through $\mathcal{P}$.

A. Photon spectrum and cross sections

As a fiducial case, we consider neutralino dark matter in order to determine an appropriate value for $\mathcal{P}$. Neutralino annihilation to a photon final state occurs via: (1) loop diagrams to two photons ($\gamma\gamma$), each of energy $E_{\gamma\gamma} = M_\chi$; (2) loop diagrams to a photon and a Z^0 boson (γZ^0) with a photon energy of $E_{\gamma Z^0} = M_\chi[1-(M_{z^0}/2M_\chi)^2]$; and (3) through an intermediate state that subsequently decays and/or hadronizes, yielding photons (h). For this latter case, the resulting photon spectrum is a continuum and is well approximated by [12]

$$\frac{dN_{\gamma,h}}{dE} = \alpha_1\frac{E}{M_\chi}\left(\frac{E}{M_\chi}\right)^{-3/2}\exp\left[-\alpha_2\frac{E}{M_\chi}\right], \tag{4}$$

where $(\alpha_1, \alpha_2) = (0.73, 7.76)$ for WW and Z^0Z^0 final states, $(\alpha_1, \alpha_2) = (1.0, 10.7)$ for $b\bar{b}$, $(\alpha_1, \alpha_2) = (1.1, 15.1)$ for $t\bar{t}$, and $(\alpha_1, \alpha_2) = (0.95, 6.5)$ for $u\bar{u}$. The cross sections associated with these processes span many orders of magnitude. For the direct annihilation to a $\gamma\gamma$ or γZ^0 final states the maximum presently allowed value of the annihilation cross section to these final states is roughly $\sim\langle\sigma v\rangle_{\gamma\gamma,\gamma Z^0} \sim 10^{-28}$ cm^3 s^{-1}. The total cross section associated with photon emission from the hadronization of the annihilation products has a corresponding upper bound of $\langle\sigma v\rangle_h \approx 5\times10^{-26}$ cm^3 s^{-1}. In the most optimistic scenario, where the cross sections are fixed to their highest value and the mass of the neutralino is ~ 46 GeV, so that $\mathcal{P} = \mathcal{P}_{\rm SUSY} \approx 10^{-28}$ cm^3 s^{-1} GeV^{-2}.

The value of $\mathcal{P}$ will be different for different dark matter candidates. For example, in models of minimal universal extra dimensions, the annihilation cross section and the mass of the lightest Kaluza-Klein particle can be significantly higher than what we assumed here (e.g., $M_\chi \gtrsim 800$ GeV [36]). However, we emphasize that our results, which constrain the density structure of dSph's (and therefore $\mathcal{L}$) can be rescaled to any dark matter candidate that annihilates to photons, by simply multiplying predicted fluxes from this work with $\mathcal{P}/\mathcal{P}_{\rm SUSY}$.

B. Dark matter distribution

Dissipationless N-body simulations show that the density profiles of CDM halos can be characterized as

$$\rho(\tilde{r}) = \frac{\rho_s}{\tilde{r}^{\gamma}(1+\tilde{r})^{\delta-\gamma}}; \qquad \tilde{r} = r/r_s, \tag{5}$$

where r_s and ρ_s set a radial scale and density normalization and γ and δ parametrize the inner and outer slopes of the distribution. For field halos, the most recent high-resolution simulations find $\delta \approx 3$ works well for the outer slope, while $0.7 \lesssim \gamma \lesssim 1.2$ works well down to $\sim 0.1\%$ of halo virial radii [34,35]. It is currently unknown whether there is a "universal" γ for every halo or if there is a scatter in γ from halo-to-halo. The range quoted here characterizes the uncertainty in the theoretical prediction for the small-r slope, and certainly provides a conservative range for the halo-to-halo scatter in central slope as well.

The structure quantity $\mathcal{L}$ that sets the annihilation flux depends primarily on the r_s and ρ_s parameters for this range of γ (see discussion below) and is even less sensitive to δ. In what follows, we will fix $\gamma = 1$ and $\delta = 3$ and derive empirical constraints on the (more important) parameters ρ_s and r_s. Note that CDM simulations also predict a specific relationship between ρ_s and r_s for halos [e.g. [37,38]] and this prediction is at least as robust as the overall shape of the profile. At the end of the next section, we compare our direct empirical constraints on the relationship between ρ_s and r_s to the expected relationship predicted from CDM simulations and use this to further tighten our constraints on the dark matter structure in the dSphs.

With $\gamma = 1$ and $\delta = 3$ the profile given in Eq. (5) is the NFW profile and we adopt this form as the basis for our constraints. With the asymptotic slopes fixed, the values of r_s and ρ_s define the profile completely. Any other nondegenerate pair of halo parameters also suffice to characterize an NFW halo. For example, halo concentration ($c \equiv R_{\rm v}/r_s$) and virial mass (M) define the profile as well. This is a less physically relevant pair for our purposes because the virial mass is set by determining the extrapolated radius, $R_{\rm v}$, within which the overdensity is equal to the virial density, $\rho_{\rm v} \simeq 100\rho_{\rm crit}$ [39]. Given c and M, the value of ρ_s is determined as $\rho_s = \rho_{\rm v} c^3/f(c)$ with $f(c) \equiv \ln(1+c) - c/(1+c)$. A second pair of parameters with perhaps more physical relevance is $V_{\rm max}$ and $r_{\rm max}$. These correspond to the maximum circular velocity curve, $V_c(r) = \sqrt{GM/r}$, and the radius where the maximum occurs. $V_{\rm max}$ is often adopted as the most direct characterization of the potential well depth of a dark matter halo, especially in the case of substructure.

Assuming a (smooth) NFW profile, the $\mathcal{L}$ term in Eq. (2) becomes

$$\mathcal{L}(\rho_s, r_s, \mathcal{D}) = 2\pi\rho_s^2 r_s^3 \int_0^{\theta_{\rm max}} \sin\theta \left\{ \int_{\rm LOS} \frac{ds}{\tilde{r}^2(\theta, \mathcal{D}, s)[1+\tilde{r}(\theta, \mathcal{D}, s)]^4} \right\} d\theta, \tag{6}$$

where $\tilde{r}(\theta, \mathcal{D}, s) = \sqrt{\mathcal{D}^2 + s^2 - 2s\mathcal{D}\cos\theta}/r_s$, the angle $\theta_{\rm max}$ defines the solid angle over which the line-of-sight (LOS) integral is performed $\Delta\Omega = 2\pi(1-\cos\theta_{\rm max})$. In the particular case where a dark matter halo is at a distance $\mathcal{D} \gg r_s$, such as the case of subhalos within a dSph, we can rewrite Eq. (6) as

$$\begin{aligned}\mathcal{L}(\rho_s, r_s) &= \int_0^{\tilde{r}_{\rm max}(\Delta\Omega, \mathcal{D})} \frac{\rho_s^2 r_s^3}{\tilde{r}^2(1+\tilde{r})^4} d^3\tilde{r}, \\ &= \frac{4\pi}{3}\rho_s^2 r_s^3 \left\{1 - \frac{1}{[1+\tilde{r}_{\rm max}(\Delta\Omega, \mathcal{D})]^3}\right\}.\end{aligned} \tag{7}$$

For an NFW profile, 90% of the flux comes within the region $\tilde{r} \le 1$. If the angular extent of r_s is less than the solid angle of interest, i.e., $\tan^{-1}[r_s/\mathcal{D}] \le \cos^{-1}[1 - \Delta\Omega/2\pi]$, Eq. (7) reduces simply to

$$\mathcal{L}(\rho_s, r_s) = \frac{7\pi}{6}\rho_s^2 r_s^3. \tag{8}$$

Typical values of the field of view of γ-ray telescopes are $\sim 10^{-2}$ steradians for atmospheric Čerenkov telescopes, and ~ 2.5 sr for space-based observatories (GLAST), with angular resolutions of ~ 1 and ~ 10 arcminutes, respectively. Note that a change in the central density profile slope γ will manifest itself as a change in the normalization of the $\rho_s^2 r_s^3$ term Eq. (8). For example, if the inner slope is as high as $\gamma = 1.2$, then $\mathcal{L}$ will be a factor of ~ 5.6 higher than what is stated in Eq. (8). If the profile is as shallow as $\gamma = 0.7$, then $\mathcal{L}$ is smaller by a factor of ~ 6.8.

C. Substructure and density profiles

Dark matter halos form hierarchically, so it is expected that they all contain some degree of gravitationally bound substructure [40–44]. The issue of dark-halo substructure, or "subhalos," is important for annihilation signals from dSphs for two reasons. First, the dark matter halos of the dSphs are subhalos, as they orbit within the virial radius of Milky Way's dark matter halo. We might expect this to have important implications for their density structure. Second, dSphs themselves are also expected to contain abundant substructure. This "sub-subhierarchy" should, in principle, continue until we reach the low-mass cutoff scale in the subhalo mass function, $m_0 \sim [10^{-13}\text{–}10^{-2}]\mathrm{M}_\odot$, which is approximately set by the CDM particle free-streaming scale [45–50]. In this case, we might expect significant enhancement of the annihilation signal compared to the "smooth" halo assumption.

Depending on the time of accretion and orbital evolution, a subhalo will experience varying degrees of mass loss as a result of tidal interactions with the *host* dark matter halo potential. Simulations suggest that the majority of the stripped material will be from the outer parts of halos. The outer slope δ of subhalo density profiles will become steeper than those of field halos. However, the interior slope, γ, will not be altered significantly [51]. Thus, our adopted NFW parametrization for the dSph dark matter density profiles is a reasonable one for determining the structure factor in the annihilation signal. The outer density profile slope does not affect the expected annihilation signal and the inner slope is expected to remain unchanged by tidal mass loss.

It is important to note that while the central slope γ is not expected to change as subhalos evolve, the *normalization* of the central profile does evolve, as subhalos monotonically lose mass, even from the central regions [51]. One implication of this is that the relationship between ρ_s and r_s for subhalos is altered relative to that of field halos. The most straightforward way to characterize this relationship in numerical simulations is to compare the $V_{\rm max}$-$r_{\rm max}$ relationship for subhalos to field halos, and it is found that subhalos tend to have smaller $r_{\rm max}$ values at fixed $V_{\rm max}$ such that $(r_{\rm S}/r_{\rm F}) \simeq 0.7(V_{\rm S}/V_{\rm F})^{1.35}$ [52,53] (see also [51,54]), where the subscripts S and F denote stripped and field quantities. As halos orbit within their parent potentials, they become less dense *and* their scale radii tend to shrink as a result of tidal interactions. We include this possibility when we compare our *empirical* constraints on the dSph density profiles to CDM expectations below.

D. Substructure and flux enhancement

Equation (6) assumes that the structure quantity $\mathcal{L}(M)$ in the γ-ray flux is set by a smoothly distributed dark matter halo of mass M. Given the expectation for substructure, a more realistic formulation is that $\mathcal{L}(M)$ is set by a smooth halo component, $\tilde{\mathcal{L}}(M)$ (set by Eq. (6)), *plus* a substructure component, that acts to enhance the flux above the smooth component expectation. It is useful to quantify this substructure component by introducing a "boost" factor B:

$$\mathcal{L}(M) = [1 + B(M, m_0)]\tilde{\mathcal{L}}(M). \tag{9}$$

We have defined the boost such that $B = 0$ is a case with no substructure and where all of the emission is from a smooth halo. The boost depends on the host dark matter halo mass M and, in principle, on m_0, the fundamental subhalo cutoff scale.

The value of B is determined by the integrated annihilation factors $\mathcal{L}(m)$ for subhalos of mass m within the host: $B\tilde{\mathcal{L}}(M) = \int (dN/dm)\mathcal{L}(m)dm$, where we have introduced the subhalo mass function dN/dm. Unfortunately a brute-force determination of B from numerical simulations is not feasible at this time because the subhalos themselves will be filled with sub-subhalos, and this progression continues until the CDM cutoff scale m_0 becomes important. This requires a dynamic range of $\sim$13 orders of magnitude in halo resolution, which is far from the current state of the art dynamical range of numerical simulations.

Our goal is to determine the expected range for B, as well as its dependence on m_0. We rely on the fact that subhalos tend to be less dense than halos in the field of the same mass. More specifically, consider the case of a subhalo that has experienced significant mass loss, such that *now* it has a maximum circular velocity $V_{\rm max} = V_{\rm S}$ that occurs at a radius $r_{\rm max} = r_{\rm S}$. In cases of significant stripping, the density profile will decline rapidly beyond $r_{\rm max}$ [e.g. [51]] and the *total* subhalo mass will be well approximated as $m_{\rm S} \simeq r_{\rm S}V_{\rm S}^2/G$. Compare this object to a field halo of the *same mass*: $M_{\rm F} \simeq 10 r_{\rm F}V_{\rm F}^2/G$, where we have assumed $c \simeq 30$ such that $\sim$10% of the halo's virial mass is contained within $r_{\rm max} = r_{\rm F}$. Adopting the numerical simulation result quoted above, $(r_{\rm S}/r_{\rm F}) \simeq 0.7(V_{\rm S}/V_{\rm F})^{1.35}$, we can derive the relative sizes of the subhalo and field halo $r_{\rm max}$'s and $V_{\rm max}$'s that give them the same total mass: $V_{\rm S} \simeq 2.2V_{\rm F}$ and $r_{\rm S} \simeq 2r_{\rm F}$. At fixed mass we therefore expect $\tilde{\mathcal{L}}_{\rm S}/\tilde{\mathcal{L}}_{\rm F} \propto (r_{\rm F}/r_{\rm S})^3 \simeq 0.125 < 1$.

The above arguments, together with the fact that subhalos are expected to have less substructure than field halos of the same mass [40,55], allow us to obtain a *maximum* estimate for B by conservatively assuming that the total structure factor $\mathcal{L}$ for a subhalo is the same as that for a host halo of the same mass: $\mathcal{L}_{\rm S}(m) = \mathcal{L}_{\rm F}(m) \equiv \mathcal{L}(m)$. Suppressing the m_0 dependence in B, this allows us to write

$$B(M) = \frac{1}{\tilde{\mathcal{L}}(M)} \int_{m_0}^{M} \frac{dN}{dm}\mathcal{L}(m)dm \tag{10}$$

$$= \frac{1}{\tilde{\mathcal{L}}(M)} \int_{m_0}^{M} \frac{dN}{dm}[1 + B(m)]\tilde{\mathcal{L}}(m)dm \tag{11}$$

$$= \frac{AM}{\tilde{\mathcal{L}}(M)} \int_{\ln m_0}^{\ln qM} [1 + B(m)]\tilde{\mathcal{L}}(m)\frac{d\ln m}{m}. \tag{12}$$

In the last step we have used the fact that the substructure mass function, dN/dm, is fairly well quantified from N-body simulations to be a power law $dN/d\ln m = A(M/m)^{\alpha}$ for $m < qM$, with $\alpha = 1$ and $q \simeq 0.1$ [56]. $q < 1$ quantifies the fact that the subhalo mass function cannot extend to the mass of the host itself. The normalization A is set by requiring a fraction f of the host mass M to be in subhalos with mass in the range $gM \leq m \leq qM$. Motivated by numerical simulations [43] and semianalytic studies [40,41] we use $f \approx 0.1$, and $g \approx 10^{-5}$ to obtain $A = f/\ln(q/g) \approx 0.01$ for $\alpha = 1$.

To estimate the mass dependence of $\tilde{\mathcal{L}}$, we use the ρ_s-r_s relation for subhalos from the model of Bullock *et al.* [38] for field halos in a standard ΛCDM cosmology. As field halos are expected to be more concentrated this will overestimate $B(M)$ and is thus a conservative assumption. This gives $c \approx 33(M/10^8 {\rm M}_\odot)^{-0.06}$ for halos of mass $M \lesssim 10^8 {\rm M}_\odot$. Using the approximation $f(c) = \log(1 + c) - c/(1 + c) \approx 2.6(c/33)^{0.4}$, and that $\rho_s \sim c^3/f(c)$, we have $\mathcal{L} \propto \rho_s^2 r_s^3 \propto Mc^{2.2} \propto M^{0.87}$.

We could solve for $B(M)$ numerically with the boundary condition that $B(m_0) = 0$. However, there is a simpler way that provides an analytic estimate for $B(M)$. We note that if the upper limit of the last integral in Eq. (12) is extended to M, then we will have an estimate that will be larger that the actual $B(M)$. Since our aim is to estimate how large the boost can be, this is a useful manipulation. We then differentiate Eq. (12). The resulting equation has an analytic solution such that we may write

$$B(M) < A\frac{(M/m_0)^{\alpha-\gamma'+A} - 1}{\alpha - \gamma' + A}, \tag{13}$$

where we have assumed that $\gamma' \equiv d\ln(\tilde{\mathcal{L}})/d\ln(M)$ is a constant. The subhalo mass function will flatten off at smaller masses and hence this, again, is a conservative assumption. Note that we have imposed the boundary condition $B(m_0) = 0$. This does not result in $B(M)$ depending sensitively on m_0 because $\alpha - \gamma' + A \simeq 0.13$ is small. For a $10^8 \mathrm{M}_\odot$ dark halo, $B(M) < 41$ if we choose $m_0 = 10^{-13}\mathrm{M}_\odot$, while $B(M) < 2$ if we choose $m_0 = 10^{-2}\mathrm{M}_\odot$.

III. MODELING OF DWARF SPHEROIDAL GALAXIES

Twenty galaxies can be classified as residing in subhalos of the Milky Way, and 18 of these are classified as dSphs. Of the 18 dSphs, nine were discovered within the last two years star counts [see e.g. [57]] and have very low luminosities and surface brightnesses. We consider six of the brighter dSphs in our study: Ursa Minor, Draco, Sculptor, Fornax, Carina, and Sextans. All of these galaxies have measured velocity dispersion profiles based on the line-of-sight velocities of ~200 stars, which may be used to constrain their dark matter halo potentials. The three remaining bright dSphs are Leo I, Leo II, and Sagittarius. Both Leo I and Leo II are too far from the Milky Way (~ 250 kpc and 205 kpc, respectively) to be detectable with γ-rays, and in the case of Leo II no velocity dispersion profile is published to our knowledge. Additionally, we do not consider Sagittarius, as this galaxy is known to be undergoing tidal stripping [58].

We assume the dSph systems to be in equilibrium and spherically symmetric. Under these assumptions, the radial component of the stellar velocity dispersion, σ_r, is linked to the total gravitational potential of the system via the Jeans equation,

$$r\frac{d(\rho_\star \sigma_r^2)}{dr} = -\rho_\star(r)V_c^2(r) - 2\beta(r)\rho_\star\sigma_r^2. \tag{14}$$

Here $\rho_\star$ is the stellar density profile, the circular velocity is $V_c(r) = GM/r$, and the parameter $\beta(r) = 1 - \sigma_r^2/\sigma_t^2$ characterizes the difference between the radial and tangential velocity dispersions. Taking β to be independent of radius and integrating σ_r^2 along the line of sight gives the velocity dispersion as a function of projected radius, R, [59]

$$\sigma_{\mathrm{LOS}}^2(R) = \frac{2}{I(R)}\int_R^\infty \left(1 - \beta\frac{R^2}{r^2}\right)\frac{\rho_\star\sigma_r^2 r}{\sqrt{r^2 - R^2}}dr. \tag{15}$$

Here, $I(R)$ is the projected surface density of the stellar distribution. In Eq. (15), σ_r depends on the mass distribution of the dark matter, and thus the parameters in the NFW profile ρ_s and r_s.

The surface density of stars in all dSphs are reasonably well fit by a two-component, spherically symmetric King profile [60],

$$I(R) = k\left[\left(1 + \frac{R^2}{r_c^2}\right)^{-1/2} - \left(1 + \frac{r_t^2}{r_c^2}\right)^{-1/2}\right]^2, \tag{16}$$

where r_t and r_c are fitting parameters denoted as the tidal and core radii (see Table I), and k is a normalization constant. The spherically symmetric stellar density can be obtained with an integral transformation of the surface

TABLE I. Properties of the dSphs used in this study. The adopted distance to each galaxy is shown in the second column. For reference, the third and fourth columns list the luminosity and central velocity dispersion for each dwarf. The fifth and sixth columns give the King core and tidal radii as determined from Refs. [61–66]. The last column shows a derived result: the range of halo $V_{\max}$ values that simultaneously matches the observed velocity dispersion profiles and the CDM theoretical normalization priors (see Fig. 2).

dSph	$\mathcal{D}$ [kpc] from [20]	L_V (10^6 $\mathrm{L}_\odot$) from [20]	σ_0 [km s^{-1}]	r_c [kpc]	r_t [kpc]	$V_{\max}$ [km s^{-1}]
Ursa Minor	66	0.29	15 ± 4	0.30	1.50	15–40
Draco	80	0.26	5.5 ± 1.2	0.18	0.93	15–35
Sculptor	79	2.2	8.5 ± 1.0	0.28	1.63	11–19
Fornax	138	15.5	11.1 ± 2.5	0.39	2.71	19–36
Carina	101	0.43	6.8 ± 1.0	0.25	0.86	10–15
Sextans	86	0.50	5.8 ± 1.3	0.40	4.0	6–10

density,

$$\rho_\star(r) = \frac{k}{\pi r_c[1+(r_t/r_c)^2]^{3/2}} \frac{1}{z^2}\left[\frac{1}{z}\cos^{-1}z - \sqrt{1-z^2}\right], \tag{17}$$

where $z^2 = (1 + r^2/r_c^2)/(1 + r_t^2/r_c^2)$.

Recent reductions of the photometric sensitivity in the extreme outer portions of dSphs show the surface density to be falling off less sharply than expected from the above King profile; outside of a "break" radius the surface density falls off like a power law $I(R) \propto R^{-2}$ [61–63]. Including these variations from the King profile has negligible effects on the results, therefore for simplicity we assume the spherically symmetric King profile for all dSphs. We note that for the particular case of Draco, recent studies have used a Plummer instead of a King profile, as described in [67]. Using a Plummer profile has no effect to this calculation, because the primary difference in the fits is in the outer regions of Draco where the surface density is exponentially declining.

In order to estimate the total mass in stars and its contribution to the total gravitational potential, we need to determine the typical range of stellar mass-to-light ratios for dSphs. Draco was considered in Lokas *et al.* [68], where they quote an upper limit to the stellar mass-to-light ratio of ~3, implying a total stellar mass of $\sim 6.6 \times 10^5 M_\odot$. Though the stellar populations vary somewhat in all dSphs, the stellar mass-to-light ratios are similar [20]. This is at the very least an order of magnitude below the deduced total mass in dark matter in all cases (see below).

There are three empirically unconstrained parameters which determine the observed line-of-sight profile in Eq. (15): β, ρ_s, and r_s. To determine the constraints on these parameters, for each dSph we construct a Gaussian likelihood function, $L \propto \exp(-\chi^2)$, where $\chi^2 = \sum_\imath(\sigma_\imath^2 - \sigma_{\mathrm{th},\imath}^2)/2\epsilon_\imath^2$. Here $\sigma_{\mathrm{th},\imath}$ is the theoretical velocity dispersion, $\sigma_\imath$ the measured dispersion in the $\imath$th bin, and $\epsilon_\imath$ is the error on $\sigma_\imath$. The assumption of a Gaussian likelihood function on the velocity dispersion is an excellent description of the data for ~200 line-of-sight velocities [69]. To construct the allowed region, we determine the χ^2 for each dSph as a function of the three parameters β, ρ_s, and r_s. Including γ as a free parameter has minimal effect on the shape of the allowed region, as long as γ is restricted in the range 0.7–1.2 [69]. Given L, we then integrate over the appropriate range of β to obtain the two-dimensional likelihood function, L', which we use to define the likelihood ratio $\Delta\chi^2 = -2\ln(L'/L'_{\max})$. We determine the allowed region in the ρ_s-r_s plane using $\Delta\chi^2 = 6.2$, equivalent to the approximate 95% confidence level region for 2 degrees of freedom.

Figure 1 shows an example fit for Ursa Minor, where we have used $\beta = 0.6$. The short-dashed curve has a maximum circular velocity, $V_{\max} \sim 70\ \mathrm{km\,s^{-1}}$, and the long-dashed curve has $V_{\max} \sim 20\ \mathrm{km\,s^{-1}}$. These correspond to $r_{\max} \sim 0.6$ kpc and ~20 kpc, respectively. This particular example highlights the degeneracy that currently exists with the line-of-sight velocity dispersion data: large $V_{\max}$ solutions are still viable as long as they are accompanied by an increase in the $r_{\max}$.

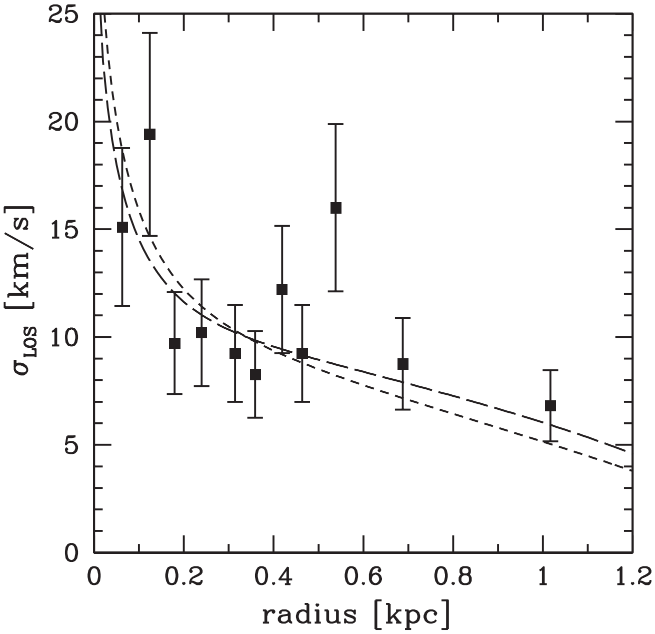

FIG. 1. The velocity dispersion profiles for Ursa Minor, with data from [61]. The short-dashed curve shows a model with $\rho_s = 10^8 M_\odot\ \mathrm{kpc}^{-3}$ and $r_s = 0.63$ kpc, while the long-dashed curve depicts a model with $\rho_s = 10^7 M_\odot\ \mathrm{kpc}^{-3}$ and $r_s = 3.1$ kpc. Both curves have $\beta = 0.6$.

Figure 2 shows the allowed regions in the ρ_s-r_s plane for each dSph. In all of the galaxies, the minima in χ^2 is not very well defined; there is a degeneracy along the axis of the allowed region. This is particularly true for the cases where the best-fitting value of r_s occurs outside the region probed by the stellar distribution. In this region, changes to the combination of ρ_s-r_s have very little impact on the dark matter distribution in the region probed by the stars, so the allowed region actually extends well beyond what is shown in the Fig. 2. We note that if the contours are created for fixed values of β, then as the value of β is changed, the ρ_s and r_s allowed region shifts *along the line of degeneracy* [e.g. [70]]. Thus our predicted $\mathcal{L}$ contribution changes very little whether we keep β fixed or marginalize over it (as we have done), especially when we demand consistency with the CDM model expectation for the ρ_s-r_s relation (see below).

Though Fig. 2 shows that the combination ρ_s-r_s is not well defined, in all of the cases the data does approximately fix the density at the mean radii $r_\star$ of the stellar distribution [69]. Calculating the total mass of the dark matter within this characteristic radius, for all galaxies the minimum implied dark matter mass $\sim 10^7 M_\odot$, which occurs for the lowest implied values of ρ_s-r_s in each case. This is at least

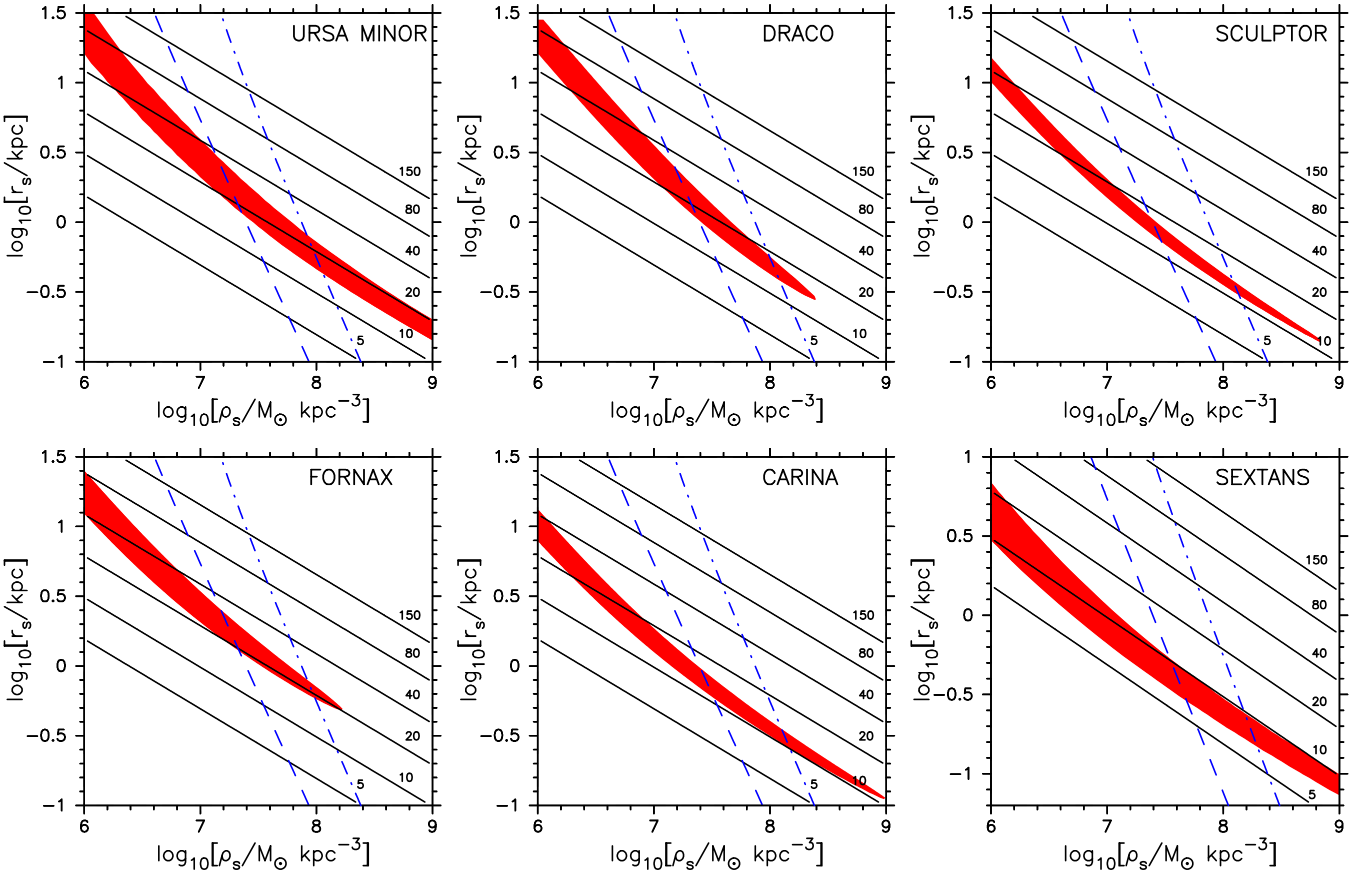

FIG. 2 (color online). The allowed region in the ρ_s-r_s plane for the six dSphs after marginalizing over the stellar velocity dispersion anisotropy parameter β. Solid lines correspond to contours with V_{max} of 5, 10, 20, 40, 80, 150 $\mathrm{km\,s^{-1}}$. Long-dashed lines represent the ρ_s-r_s relation as derived from the field halo relation, and the 2-σ scatter above the median concentration vs mass relation. Dot-dashed lines represent the ρ_s-r_s relation as derived from the tidally stripped halo relation, and the 2-σ scatter below the median concentration vs mass relation.

an order of magnitude greater than the contribution to the total mass in stars in all cases.

Over-plotted in Fig. 2 are lines of constant V_{max} in the ρ_s-r_s plane. Phrasing the dark matter halo properties in terms of V_{max} allows for a direct comparison to CDM models, which provide predictions for the cumulative number distribution of halos at a given V_{max}. Although the high V_{max} solutions are plausible by considering the data alone, comparison to CDM models show that it is improbable that all of these halos have V_{max} in the high end of the allowed regime [40,70–72] (although this solution may be viable for some smaller fraction [73]). Typical CDM halos have $\sim$1 system as large as $\sim$60 $\mathrm{km\,s^{-1}}$.

Dashed and dash-dotted lines in Fig. 2 enclose the predicted ρ_s-r_s relation (including scatter) for cold dark matter halos as determined from numerical simulations. In order to provide a conservative range for the CDM expectation, the upper (long-dashed) lines are obtained using the relation that is 2-σ *above* the median for field halos in ΛCDM [38] and the lower (dash-dotted) lines show the relation implied by the tidally stripped V_{max}-r_{max} relation with a 2-σ scatter *below* the median $c(M)$ relation [52,53]. We consider both the field and stripped relation because the degree of tidal stripping experienced by each dSph is uncertain, depending sensitively on the precise orbital information and/or redshift of accretion, two quantities that set the amount of tidal mass loss [40]. The region where the CDM predictions cross with the observationally allowed values of ρ_s and r_s in Fig. 2 defines a preferred model for the structure of these dark matter halos within the context of CDM.

IV. FLUXES FROM DWARF SPHEROIDAL GALAXIES

A. Smooth halo

The flux of γ-rays originating from the annihilation of dark matter particles is sensitive to $\rho_s^2 r_s^3$ (recall that $\mathcal{L} \sim \rho_s^2 r_s^3$, see also Eq. (6)). Even though ρ_s and r_s individually can vary by orders of magnitude and still satisfy the observed velocity dispersion profile (see Fig. 2), the product $\rho_s^2 r_s^3$ is tightly constrained. Figure 3 shows the allowed

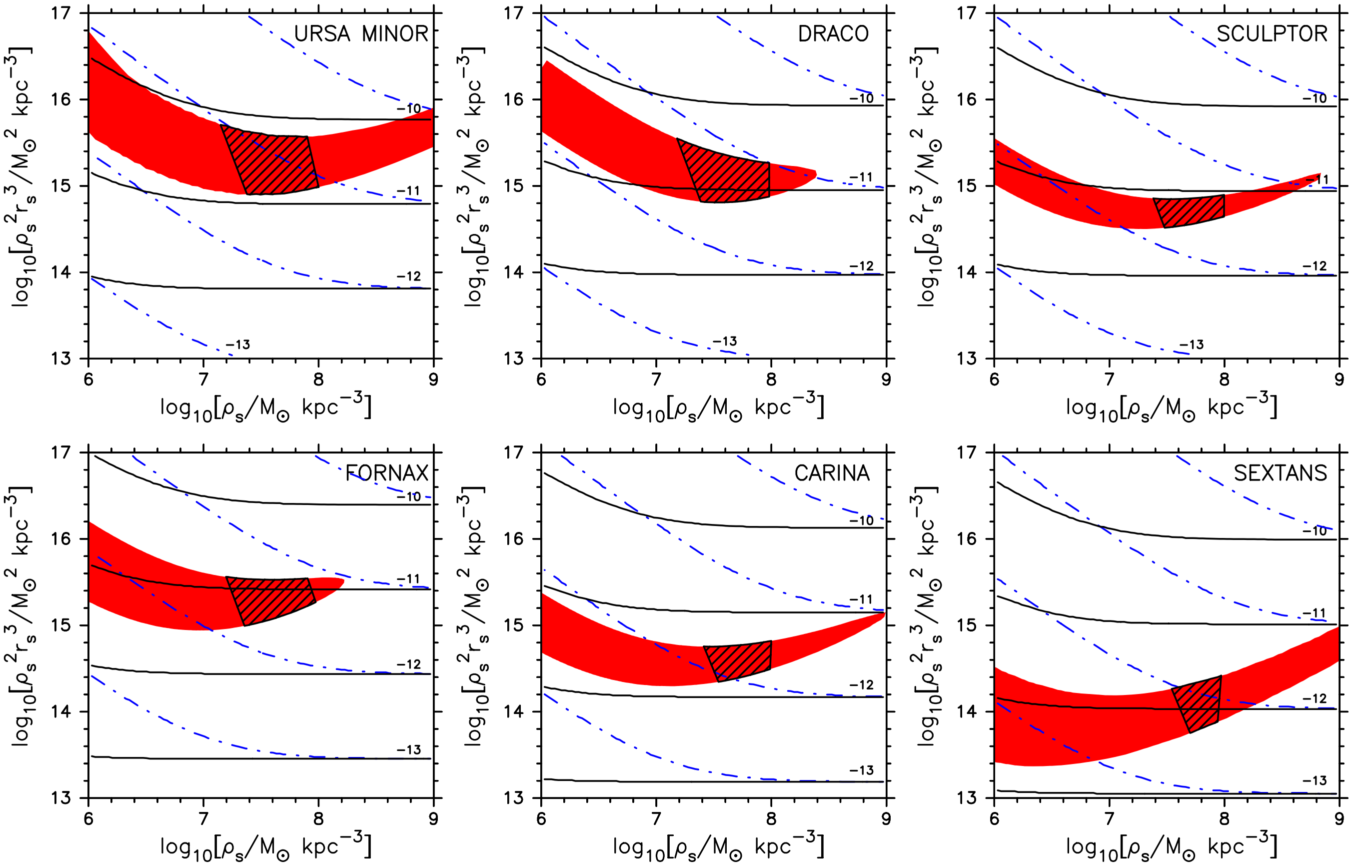

FIG. 3 (color online). The allowed region in the $\rho_s^2 r_s^3$-ρ_s plane for each dSph after marginalizing over the stellar velocity dispersion anisotropy parameter β filled region, and contour levels for the expected γ-ray flux. Contours are shown for $\log_{10}[dN_\gamma/dAdt] = -13$, -12, -11, and -10, where the flux is measured in photons $\mathrm{cm}^{-2}\ \mathrm{s}^{-1}$. Solid contours depict the flux expected within a region of radius 2 degrees centered on the dwarf, while dot-dashed contours depict the same flux thresholds for a region of radius 0.1° centered on the dwarf. The hatched regions represent the preferred region from CDM theoretical modeling (see Fig. 2 and discussion in text).

region in the $\rho_s^2 r_s^3$-ρ_s plane. The tight constraint makes the predictions for γ-ray fluxes more robust. The hatched regions correspond to solutions that overlap with the CDM expectation in this parameter space. With the CDM prior imposed, the $\rho_s^2 r_s^3$ quantity is constrained to within a factor of ~3–6 in all cases. This corresponds to the width of the hatched regions in Fig. 3.

The mild change in $\rho_s^2 r_s^3$ with ρ_s can be explained by looking at the radial velocity dispersion measure. First note that the contours in Fig. 3 have a common shape. They slope gently down for about a decade in ρ_s, remain constant, and then start to slope upwards (as ρ_s is increased). In addition the area where the contours remain roughly constant is where $r_s \sim r_t$; recall that r_t is the tidal radius of the stars. The LOS velocity dispersion is a weighted average of the radial velocity dispersion for $r < r_t$, see Eq. (15). Thus the ρ_s-r_s scaling must trace back to the scaling of $\sigma_r^2(r)$. For a constant stellar anisotropy, we have

$$\sigma_r^2(r) = \frac{G r^{-2\beta}}{\rho_\star(r)} \int_r^\infty dr' \rho_\star(r') r'^{2\beta-2} M(r'), \qquad (18)$$

where $M(r)$ is the total mass profile, which is to a good approximation the dark matter mass profile. We are interested in the scaling of $\sigma_r^2(r)$ with ρ_s and r_s. It is clear from Eq. (18) that $\sigma_r^2(r) \propto \rho_s$ always. To understand the scaling with r_s, we consider the following integral, $r_s^3 \int_r^{r_t} dr' \rho_\star(r') r'^{2\beta-2}(\ln(1 + r'/r_s) - r'/(r' + r_s))$. This integral, obtained from Eq. (18), has all the information about the scaling of $\sigma_r^2(r)$ with r_s. For $r_s \gg r_t$, the NFW mass term can be replaced with $r'^2 r_s$, which implies that $\sigma_r^2(r)$ scales as $\rho_s r_s$ for a given r, and hence we would predict that ρ_s scales as $1/r_s$ for $r_s \gg r_t$. This prediction is verified by the shape of the contours for the smaller values of ρ_s (larger values of r_s) in Figs. 2 and 3.

For $r_s \ll r_t$, the NFW mass term varies slowly compared to $\rho_\star$ and possibly the β terms. This means that $\sigma_r^2(r)$ should scale (in the above limit) as $\rho_s r_s^3$ or the contour of $\rho_s^2 r_s^3$ should increase linearly with ρ_s. We can discern this behavior for Sextans, which has a large r_t. In the intermediate region where $r_s \sim r_t$, $\sigma_r^2(r)$ varies faster than linearly with r_s. To see this, we first note that $\delta(r) \equiv d\ln M(r)/d\ln r$ is 1.3 at $r = r_s$ and is 1.8 at $r = 0.2 r_s$. Also, r_c/r_t is between 0.1 and 0.3 for these galaxies and most of the contribution to the LOS dispersion comes from the region around r_c. Therefore we expect the contours to be along curves of constant $\rho_s r_s^{3-\delta(r_c)}$, which explains the flat parts of the contours in Fig. 3 (where they overlap with the CDM priors).

The contours in the $\rho_s^2 r_s^3$-ρ_s plane in Fig. 3 have been calculated assuming a smooth dark matter distribution. The flux enhancement due to the presence of substructure will be discussed below. We have used $\mathcal{P} = \mathcal{P}_{\rm SUSY} = 10^{-28}$ cm^3 s^{-1} GeV^{-2}, which corresponds to the most optimistic scenario for neutralino CDM. For other dark matter candidates, the fluxes shown should be rescaled by a factor of $\mathcal{P}/\mathcal{P}_{\rm SUSY}$.

Figure 3 shows that the most promising candidates for detection are Ursa Minor and Draco, with the largest flux coming from Ursa Minor. These two dSphs have fluxes $\sim 10^{-11}$ cm^{-2} s^{-1}, within potential reach of upcoming γ-ray detectors. For example, the integral sensitivity for a 5-σ detection in 5 years of exposure with GLAST in the signal dominated regime (energies above ~ 5 GeV) is $\sim 3 \times 10^{-11}$ cm^{-2} s^{-1}, and therefore these two dSphs should be prime targets for observation with GLAST.

The various lines in Fig. 3 show flux levels for different solid angles of integration centered on the dSph. Because most of the flux from a dark matter halo described with an NFW profile originates from the region inside of r_s, integrating over an area that is larger than the apparent angular extent subtended by r_s does not lead to a marginal increase in the flux (see e.g. Eq. (8)). For a dSph at a distance $\mathcal{D}$ this angular extent is $\tan^{-1}[r_s/\mathcal{D}]$. Integrating over an angular area which has an apparent radius smaller than r_s leads to a reduction in flux (see e.g. Eq. (7)). This is shown with the dot-dashed contours in Fig. 3, where the solid angle is 0.1 degrees relative to the solid contours which are for 2 degrees.

In order to quantify the prospects for detection we consider the following examples. If a region of radius 0.1 degrees centered on Ursa Minor is integrated upon with GLAST (with an orbit-averaged area of $\mathcal{A}_{\rm eff} \sim 2 \times 10^3$ cm^2 [74]) for 5 years, and $\mathcal{P} \approx 10^{-28}$ cm^3 s^{-1} GeV^{-2}, then the range in the number of photons expected is $\sim$[5–35] based on the allowed range of values in the ρ_s-r_s plane. Integrating over the same region with a Čerenkov detector (such as VERITAS (atmospheric) or HAWC (water)) has the advantage of a much larger effective area ($\mathcal{A}_{\rm eff} \sim 10^8$ cm^2), but the disadvantage of a much larger background (due to the hadronization of cosmic rays) and much smaller integration time scale (of order hours instead of years). For ground detectors such as VERITAS, or HAWC, with an effective area $\mathcal{A}_{\rm eff} \sim 10^8$ cm^2, and as an example, 50 hours of integration, the corresponding range in the number of photons expected is [10–70]. For this latter estimate we assume $\mathcal{P} \approx 10^{-31}$ cm^3 s^{-1} GeV^{-2} which corresponds to a neutralino of $M_\chi \sim 200$ GeV and a threshold energy of ~ 100 GeV.

As can be inferred from Fig. 3, the predicted fluxes are roughly similar to within 2 orders of magnitude. If a γ-ray flux is detected in the direction of, for example, Ursa Minor, then from the allowed ρ_s-r_s parameter space of Ursa Minor we can determine the range of expected fluxes for the remaining five dSphs, by taking into account the respective allowed ρ_s-r_s parameter space in each case. Table II provides the flux ratios expected relative to a flux measurement from Ursa Minor. We calculate these flux ratios by considering the highest and lowest flux in the $\rho_s^2 r_s^3$-ρ_s parameter space which is also consistent with the CDM priors (shaded areas in Fig. 3). If the highest flux predicted from Ursa Minor is $\Phi_{\rm UMI}^{\rm max}$ and the minimum is $\Phi_{\rm UMI}^{\rm min}$, then the range of flux ratios from the rest dSphs relative to the flux from Ursa Minor is $\Phi_{\rm dSph}^{\rm max}/\Phi_{\rm UMI}^{\rm min} - \Phi_{\rm dSph}^{\rm min}/\Phi_{\rm UMI}^{\rm max}$. We calculate flux ratios for two different angular integrations, such that combinations of the two remove any correlations between the allowed regions by the inclusions of the distance to each dwarf, i.e., a same allowed value of $\rho_s^2 r_s^3$ in, for example, two different dSphs does not necessarily correspond to the same flux (recall that the angular extent of r_s for a dSph at D is $\tan^{-1}[r_s/D]$, and that the flux is proportional to $\rho_s^2 r_s^3$). This prediction is quite robust. First, because measurement of γ-ray fluxes must fall within the prescribed tight range in the $\rho_s^2 r_s^3$-ρ_s plane if all dSphs are composed of the same CDM particles, and second because the predicted flux ratios are less sensitive to astrophysical processes, which may contaminate the γ-ray emission. Therefore, correlated fluxes between dSphs should be expected in future measurements.

The results presented in Fig. 3 are fluxes integrated over an energy regime that contains the signal from dark matter annihilation for a fiducial value of $\mathcal{P}$. Extraction of a signal from dark matter annihilation will depend on the shape of both the input and the background spectra. In Fig. 4, we show an example of the spectrum from dark matter annihilations in Ursa Minor,

$$E^2 \frac{dN_\gamma}{dAdtdE} = 5 \times 10^{-12}\ \text{GeV cm}^{-2}\ \text{s}^{-1} E^2 \frac{dN_\gamma}{dE} \times \left[\frac{\sigma v}{5 \times 10^{-26}\ \text{cm}^3\ \text{s}^{-1}}\right]\left[\frac{46\ \text{GeV}}{M_\chi}\right]^2 \times \left[\frac{B+1}{1}\right]\left[\frac{\mathcal{L}(\rho_s, r_s, \mathcal{D})}{1.25 \times 10^{15}\ \text{GeV}^2\ \text{cm}^{-5}}\right]. \quad (19)$$

TABLE II. The predicted flux ratios for dSphs relative to the γ-ray flux from Ursa Minor in CDM theory.

dSph	Within 0.1 deg	Within 2 deg
Draco	0.1–3.2	0.1–2.8
Sculptor	0.07–1.6	0.05–0.7
Fornax	0.07–2.2	0.05–1.1
Carina	0.04–1.0	0.02–0.4
Sextans	0.02–0.5	0.007–0.02

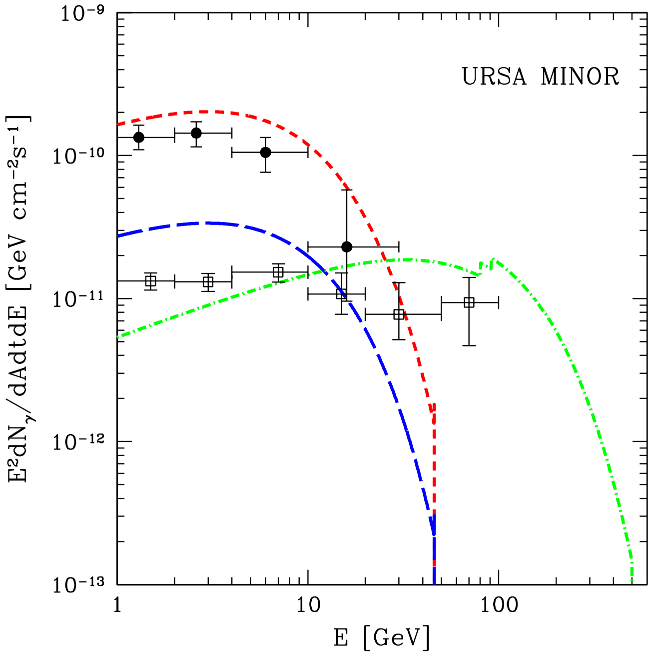

FIG. 4 (color online). Examples of the flux spectrum of Ursa Minor for three cases where the quantities ($\log_{10}\rho_s$, $\log_{10}r_s$, M_χ) take the values of (7.4, 0.033, 46) depicted with the long-dashed line, (7.9, −0.067, 46) shown as a short-dashed line, and (7.9, −0.067, 500) shown as the dot-dashed line. The value of $\mathcal{L}$ that corresponds to these 3 cases is [2.08×10^{14}, 1.25×10^{15}, 1.25×10^{15}] GeV cm^{-2} s^{-1}, respectively. The units for ρ_s are $M_\odot$ kpc^{-3}, while r_s is in kpc and M_χ in GeV. No enhancement of flux from substructure is included; substructure could increase the flux by up to a factor of 100, increasing the prospects for detection. The calculated flux is integrated over an angular region of radius 0.1 degrees centered on the dSph, and the value of $\mathcal{P} = \mathcal{P}_{\rm SUSY} \approx 10^{-28}$ cm^3 s^{-1} GeV^{-2}, which corresponds to the most optimistic scenario for supersymmetric dark matter (see Sec. II). Open squares show the amplitude of the γ-ray extragalactic emission [75], while filled circles correspond to the galactic emission of γ-rays at high galactic latitudes [76].

The assumed values of ρ_s and r_s in this example are consistent with the observed velocity dispersion-derived profile, and also with the predictions of CDM theory (see Fig. 2). This highlights the range of values that the amplitude of the spectrum may take. As shown in Fig. 3, the structure quantity $\mathcal{L}$ can be a factor of 3 greater, or a factor of 2 smaller than what is assumed in this example. On the other hand, the cross section assumed represents an upper bound for the continuum emission of γ-rays from the hadronization of the annihilation products, and can be smaller by up to 6 orders of magnitude, while the mass of the dark matter particle represents the lower experimental bound for neutralino dark matter. Note that the boost factor B in this particular example is taken to be 0. We will discuss this in the next section.

In Fig. 4 we show the spectrum of photon emission from within an angular region of 0.1 degrees for different choices of the values of ρ_s, r_s, and M_χ. Shown are also the γ-ray background spectrum that have extragalactic [75] and galactic [76] origin. Increasing the angular acceptance of a detector from 0.1 degrees to radii larger than the projected angular size of r_s does not lead to a significant increase in the flux from the dSph, but it does increase considerably the flux from the two diffuse components. This can be understood in the following way. For an NFW profile, the majority of flux originates from the region within r_s. The distance to Ursa Minor is $\mathcal{D} = 66$ kpc, and therefore the observed angular extent of the scale radius of Ursa Minor is $\tan^{-1}[r_s/\mathcal{D}] \approx 0.7$ degrees. Thus, integrating over a region greater than 0.7 degrees does not lead to a substantial increase in the flux. On the other hand, we can find the decrease in the measured flux that results from an integration over an area smaller than the angular extent of r_s, say, 0.1 degrees. In this case, we use Eq. (7), and find that the emitted flux should be a factor of ≈ 1.7 less than the value obtained by integrating out to 0.7 degrees.

TABLE III. The CDM-predicted angular extent in degrees where at least 90% of the γ-ray flux should originate for each dSph.

dSph	Radius of the area of 90% flux emission in degrees
Ursa Minor	0.4–2.7
Draco	0.3–1.8
Sculptor	0.2–0.9
Fornax	0.2–1.0
Carina	0.1–0.6
Sextans	0.1–0.4

We therefore emphasize that increasing the area of integration does not significantly increase the flux from the dSph as long as it is of order or larger than $\tan^{-1}[r_s/\mathcal{D}]$. However, increasing the integration area does increase the photon counts that originate from contaminating sources. In Table III we show the range of the angular extent in degrees where 90% of the flux will originate for each dSph. We calculate this quantity using the values of r_s consistent with CDM predictions (see Fig. 2). Future observations of the six dSphs presented here should concentrate on integrating over areas with radii as shown in Table III centered on each dSph.

B. Including substructure

In this section, we study the effect of substructure on the γ-ray flux. We assume the same constraints on the dark halos as shown in Fig. 2, and combine them with Eq. (12) in order to determine the substructure flux boost factor B introduced in Eq. (9). We will first need an estimate for the total mass of the dark halos for a given point in the ρ_s-r_s parameter space. For these estimates, we first use the Jacobi approximation to determine the tidal radius, $r_t \simeq \mathcal{D}(m(r_t)/3/M_{MW}(\mathcal{D}))^{1/3}$. Here $\mathcal{D}$ is the distance to the dSph, $M_{MW}(\mathcal{D})$ is the extrapolated mass of the Milky Way at that distance, and m is the mass of the dSph which we wish to determine. For the Milky Way mass, we use an asymptotically flat rotation curve, with $V_{\rm max} \simeq 220\ {\rm km\,s^{-1}}$. Because $\mathcal{D}$ is much larger than the typical scale radius of the Milky Way halo when fit by an NFW profile, our results are insensitive to the choice of the mass model for the Milky Way. For each galaxy, we thus solve for r_t, and then the total mass within r_t, given an input pair of ρ_s-r_s.

In the left panel of Fig. 5 we show the range of values of the substructure boost factor for each dSph, based on the allowed region from combining CDM theory and velocity dispersion data in the ρ_s-r_s parameter space (see Fig. 2). We note two important results: (1) the value of B is only weakly dependent on the cutoff scale of the subhalo mass function, and (2) the boost factor can take values which are at most of order $\sim$100 in all dSphs. We can understand these effects by recalling the solution to Eq. (13), where the boost factor of a halo of mass M (with a subhalo mass function with a cutoff at a scale m_0) is approximately given by $B(M, m_0) \approx 0.1((M/m_0)^{0.13} - 1)$. The weak dependence on m_0 is a result of the flatness of the relationship between the concentration and mass in CDM halos (which is an outcome of the flatness of the dark matter power spectrum). For scales $\sim 10^7 {\rm M}_\odot$, the concentration parameter scales with mass as $c \sim m^{-0.06}$, while for much smaller scales, e.g. $\sim 10^{-5} {\rm M}_\odot$, it becomes even shallower, $c \sim m^{-0.037}$. As such, the boost factor in dark matter halos does not increase dramatically when the cutoff in the subhalo mass function is reduced.

In the right panel of Fig. 5 we show the effect of the subhalo mass function power law to the boost factor. As an example, we use Ursa Minor, with a mass of $M = 3.02 \times 10^8 {\rm M}_\odot$, and characteristic density and radius of $\rho_s = 6.3 \times 10^7 {\rm M}_\odot\ {\rm kpc}^{-3}$ and $r_s = 0.8$ kpc, respectively. A change in the power-law index leads to significantly different behavior. For example, if the subhalo mass function has a cutoff at $10^{-5} {\rm M}_\odot$, then a 5% uncertainty in the subhalo mass function power law manifests itself into a difference in B by as much as a factor of 80. In addition, note that for a subhalo mass function $dN/d\ln m \sim m^{-\alpha}$, and a luminosity of $\mathcal{L} \sim \rho_s^2 r_s^3 \sim m^{0.87}$, the luminosity per logarithmic mass interval in substructure is $d\mathcal{L}/d\ln m \sim \mathcal{L}(m) dN/d\ln m \sim M^{0.87-\alpha}$. Therefore, for mass functions with $\alpha \sim 0.9$, the contribution to the boost factor per logarithmic mass interval is a very weak function of subhalo mass.

V. SUMMARY

We address the prospects for detecting dark matter annihilation from six dwarf spheroidal satellites of the Milky Way. Using the stellar velocity dispersion profiles for each dSph, and assuming an NFW profile for the dark matter, we deduce constraints on both the characteristic density ρ_s and characteristic radius r_s. We show that each dSph exhibits a degeneracy in the ρ_s-r_s parameter space. We have assumed that the stellar velocity dispersion has a constant anisotropy and allowed it to vary. However, the degeneracy exists even if the anisotropy is kept fixed. The ρ_s-r_s degeneracy translates to a degeneracy in the more observationally relevant parameters of $V_{\rm max}$ and the radius where the maximum rotation speed is attained $r_{\rm max}$. The degeneracy direction is such that larger values of $V_{\rm max}$ are allowed as long as they are accompanied by the corresponding increase in $r_{\rm max}$. However, this degeneracy is

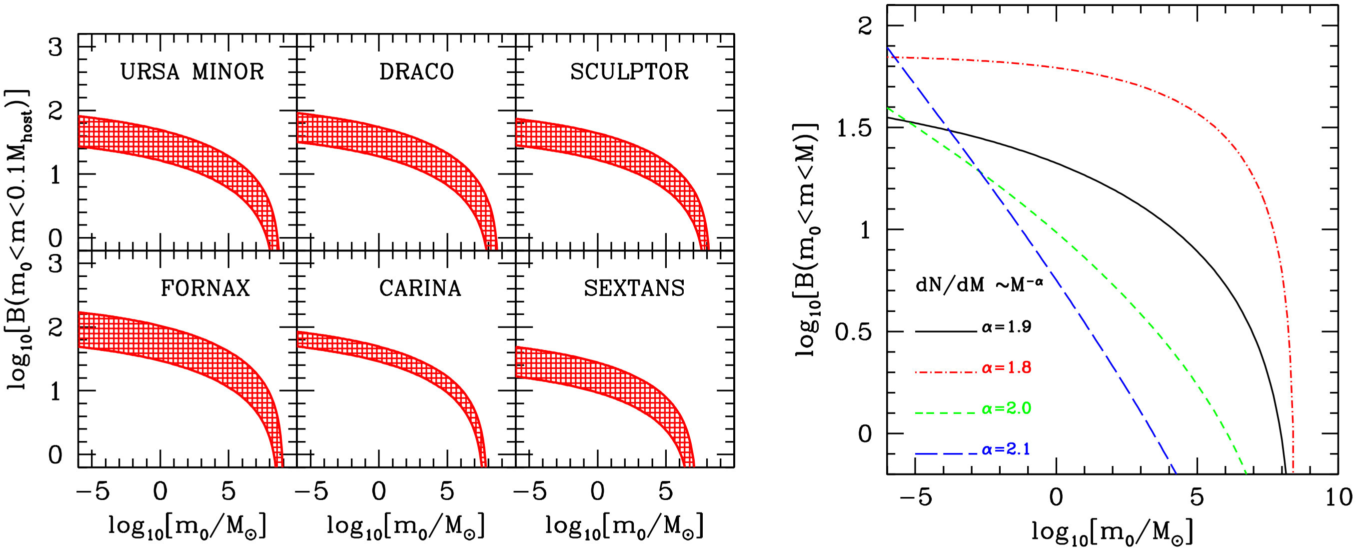

FIG. 5 (color online). Left: The predicted substructure boost factors assuming a subhalo mass function scaling as $dN/dM \sim M^{-1.9}$. Right: The dependence of the overall substructure boost factor to the slope of the subhalo mass function for Ursa Minor. The assumed parameters are $M = 3.02 \times 10^8 {\rm M}_\odot$, $\rho_s = 6.3 \times 10^7 {\rm M}_\odot\ {\rm kpc}^{-3}$, and $r_s = 0.8$ kpc.

broken substantially because in CDM theory, there is a relation between ρ_s and r_s. We find that imposing this CDM "prior" constrains $5\ \mathrm{km\,s^{-1}} < V_{\mathrm{max}} < 40\ \mathrm{km\,s^{-1}}$ in all the dSphs we consider (see Table II).

Assuming a smooth dark matter distribution in the dSph halos, we find that Ursa Minor and Draco are the most promising dSph's for detecting products of dark matter annihilation. Fornax and Sculptor are a factor of ~ 10 fainter, while Carina and Sextans are fainter by a factor of ~ 100. In the most optimistic scenario for neutralino dark matter, the largest-predicted flux from Ursa Minor is $\sim 3 \times 10^{-11}\ \mathrm{cm^{-2}\,s^{-1}}$. This is the flux within a 0.1° radius centered on Ursa Minor, and is within the sensitivity threshold of future detectors, such as GLAST [10]. Given the fact that all dSphs will have the same spectrum from dark matter annihilation, the prospects of detection may be further enhanced by stacking the signal from all 6 dSphs presented in this work. This can lead to an increase in the total flux up to a factor of 2. The flux predictions presented here can easily be rescaled to any dark matter candidate that annihilates to photons (see Sec. IV).

The dark matter distribution is certainly not smooth and the presence of rich substructure in dark matter halos can enhance the flux from annihilation of dark matter particles. We calculate this enhancement resulting from substructure, and find that it can be at most ~ 100, independent of the cutoff scale in the subhalo mass function. In the most optimistic particle physics scenario, this enhancement puts the fluxes from all the dSph's we consider above the threshold of future γ-ray detectors.

While the allowed region in ρ_s-r_s parameter space is degenerate, we show that the corresponding range in the product $\rho_s^2 r_s^3$ is much more tightly constrained. This is important because the γ-ray luminosity from dark matter annihilation is $\mathcal{L} \sim \rho_s^2 r_s^3$, implying that the range of predicted fluxes is narrow. We find that the observationally deduced values in the fluxes can vary by a factor of ~ 10 and imposing the CDM prior further reduces the uncertainty to a factor of $\sim$3–6, depending on the particular distribution of dark matter in each dSph. This range will only be reduced with the inclusion of more stars in the analysis of the line-of-sight velocity dispersion profiles.

Throughout this work, we have assumed that the dark matter density profiles are described with an inner slope of $\gamma = 1$ (NFW). Dark matter annihilation signal is proportional to the square of the density, so the predicted flux is sensitive to the value of γ. Varying the inner slope within the current theoretical uncertainty $0.7 < \gamma < 1.2$ results in a flux increase or decrease by a factor of ~ 6. It is not yet clear if the spread in γ we quote above is truly the scatter from halo to halo or if much of it reflects numerical resolution issues. If there is a distribution of values in γ as large as that quoted above, and it is independent of host halo mass, then this uncertainty will have to be factored into the flux predictions. If the inner slope correlates with mass or if the true scatter in γ from halo to halo is small, then our predictions for flux ratios are robust. Future N-body simulations will be crucial in constraining the theoretical uncertainty in γ.

ACKNOWLEDGMENTS

We would like to thank Gerard Jungman, Tobias Kaufmann, and Gus Sinnus for enlightening conversations. We are grateful to John Beacom for comments on an earlier draft of this manuscript. L. E. S. acknowledges support from the Center for Cosmology at UC Irvine. J. S. B., L. E. S., and M. K. are supported in part by NSF Grant No. AST-0607746. Work at LANL was carried out under the auspices of the NNSA of the U.S. Department of Energy at Los Alamos National Laboratory under Contract No. DE-AV52-06NA25396.

---

[1] D. N. Spergel *et al.*, arXiv:astro-ph/0603449.
[2] G. Jungman, M. Kamionkowski, and K. Griest, Phys. Rep. **267**, 195 (1996).
[3] G. Bertone, D. Hooper, and J. Silk, Phys. Rep. **405**, 279 (2005).
[4] H.-C. Cheng, J. L. Feng, and K. T. Matchev, Phys. Rev. Lett. **89**, 211301 (2002).
[5] D. S. Hanna *et al.*, Nucl. Instrum. Methods Phys. Res., Sect. A **491**, 126 (2002), http://www.astro.ucla.edu/~stacee/.
[6] W. Hofmann (HESS Collaboration), in International Cosmic Ray Conference (2003), p. 2811, http://www.mpi-hd.mpg.de/hfm/HESS/HESS.html.
[7] M. Martinez (MAGIC Collaboration), in International Cosmic Ray Conference (2003), p. 2815, http://wwwmagic.mppmn.mpg.de.
[8] T. C. Weekes *et al.*, Astropart. Phys. **17**, 221 (2002), http://veritas.sao.arizona.edu/.
[9] T. Yoshikoshi *et al.*, Astropart. Phys. **11**, 267 (1999), http://icrhp9.icrr.u-tokyo.ac.jp/.
[10] S. Ritz, J. Grindlay, C. Meegan, and P. F. Michelson (GLAST Mission Team), Bull. Am. Astron. Soc. **37**, 1198 (2005), http://glast.stanford.edu/.
[11] G. Sinnis, AIP Conf. Proc. No. 745 (AIP, New York, 2005), p. 234.
[12] L. Bergstrom, P. Ullio, and J. H. Buckley, Astropart. Phys. **9**, 137 (1998).
[13] D. Hooper and B. L. Dingus, Phys. Rev. D **70**, 113007 (2004).
[14] S. Profumo, Phys. Rev. D **72**, 103521 (2005).
[15] D. Merritt, M. Milosavljevic, L. Verde, and R. Jimenez, Phys. Rev. Lett. **88**, 191301 (2002).

[16] G. Bertone and D. Merritt, Mod. Phys. Lett. A **20**, 1021 (2005).
[17] J. A. Sellwood, Astrophys. J. **587**, 638 (2003).
[18] O. Y. Gnedin and J. R. Primack, Phys. Rev. Lett. **93**, 061302 (2004).
[19] C. Tonini and A. Lapi, Astrophys. J. **649**, 591 (2006).
[20] M. Mateo, Annu. Rev. Astron. Astrophys. **36**, 435 (1998).
[21] E. A. Baltz, C. Briot, P. Salati, R. Taillet, and J. Silk, Phys. Rev. D **61**, 023514 (2000).
[22] C. Tyler, Phys. Rev. D **66**, 023509 (2002).
[23] N. W. Evans, F. Ferrer, and S. Sarkar, Phys. Rev. D **69**, 123501 (2004).
[24] L. Bergstrom and D. Hooper, Phys. Rev. D **73**, 063510 (2006).
[25] L. Pieri and E. Branchini, Phys. Rev. D **69**, 043512 (2004).
[26] C. Calcaneo-Roldan and B. Moore, Phys. Rev. D **62**, 123005 (2000).
[27] A. Tasitsiomi and A. V. Olinto, Phys. Rev. D **66**, 083006 (2002).
[28] F. Stoehr, S. D. M. White, V. Springel, G. Tormen, and N. Yoshida, Mon. Not. R. Astron. Soc. **345**, 1313 (2003).
[29] S. M. Koushiappas, A. R. Zentner, and T. P. Walker, Phys. Rev. D **69**, 043501 (2004).
[30] E. A. Baltz, J. E. Taylor, and L. L. Wai, arXiv:astro-ph/0610731.
[31] J. Diemand, M. Kuhlen, and P. Madau, arXiv:astro-ph/0611370.
[32] L. Pieri, E. Branchini, and S. Hofmann, Phys. Rev. Lett. **95**, 211301 (2005).
[33] S. M. Koushiappas, Phys. Rev. Lett. **97**, 191301 (2006).
[34] J. F. Navarro *et al.*, Mon. Not. R. Astron. Soc. **349**, 1039 (2004).
[35] J. Diemand, M. Zemp, B. Moore, J. Stadel, and M. Carollo, Mon. Not. R. Astron. Soc. **364**, 665 (2005).
[36] L. Bergstrom, T. Bringmann, M. Eriksson, and M. Gustafsson, J. Cosmol. Astropart. Phys. 04 (2005) 004.
[37] J. F. Navarro, C. S. Frenk, and S. D. M. White, Astrophys. J. **490**, 493 (1997).
[38] J. S. Bullock *et al.*, Mon. Not. R. Astron. Soc. **321**, 559 (2001).
[39] G. L. Bryan and M. L. Norman, Astrophys. J. **495**, 80 (1998).
[40] A. R. Zentner and J. S. Bullock, Astrophys. J. **598**, 49 (2003).
[41] F. C. van den Bosch, G. Tormen, and C. Giocoli, Mon. Not. R. Astron. Soc. **359**, 1029 (2005).
[42] D. Reed, F. Governato, T. Quinn, J. Gardner, J. Stadel, and G. Lake, Mon. Not. R. Astron. Soc. **359**, 1537 (2005).
[43] J. Diemand, B. Moore, and J. Stadel, Mon. Not. R. Astron. Soc. **352**, 535 (2004).
[44] J. E. Taylor and A. Babul, Mon. Not. R. Astron. Soc. **348**, 811 (2004).
[45] C. Schmid, D. J. Schwarz, and P. Widerin, Phys. Rev. D **59**, 043517 (1999).
[46] S. Hofmann, D. J. Schwarz, and H. Stoeker, Phys. Rev. D **64**, 083507 (2001).
[47] A. M. Green, S. Hofmann, and D. J. Schwarz, Mon. Not. R. Astron. Soc. **353**, L23 (2004).
[48] A. M. Green, S. Hofmann, and D. J. Schwarz, J. Cosmol. Astropart. Phys. 08 (2005) 003.
[49] A. Loeb and M. Zaldarriaga, Phys. Rev. D **71**, 103520 (2005).
[50] S. Profumo, K. Sigurdson, and M. Kamionkowski, Phys. Rev. Lett. **97**, 031301 (2006).
[51] S. Kazantzidis, A. R. Zentner, and A. V. Kravtsov, Astrophys. J. **641**, 647 (2006).
[52] J. S. Bullock and K. V. Johnston, Astrophys. J. **635**, 931 (2005).
[53] J. S. Bullock and K. V. Johnston, in Proceedings of Island Universes: Structure and Evolution of Disk Galaxies, Baltimore, 2006, edited by R. de Jong (Springer, Dordrecht, to be published).
[54] C. Power, Ph.D. Thesis, University of Durham, 2003.
[55] L. Gao, S. D. M. White, A. Jenkins, F. Stoehr, and V. Springel, Mon. Not. R. Astron. Soc. **355**, 819 (2004).
[56] J. Diemand, M. Kuhlen, and P. Madau, Astrophys. J. **649**, 1 (2006).
[57] V. Belokurov, D. B. Zucker, N. W. Evans, J. T. Kleyna, S. Koposov, S. T. Hodgkin, M. J. Irwin, G. Gilmore, M. I. Wilkinson, and M. Fellhauer *et al.*, Astrophys. J. **654**, 897 (2007).
[58] S. R. Majewski *et al.*, Astrophys. J. **619**, 800 (2005).
[59] J. Binney and G. A. Mamon, Mon. Not. R. Astron. Soc. **200**, 361 (1982).
[60] I. King, Astron. J. **67**, 471 (1962).
[61] C. Palma *et al.*, Astrophys. J. **125**, 1352 (2003).
[62] R. R. Munoz *et al.*, Astrophys. J. **631**, L137 (2005).
[63] K. B. Westfall *et al.*, Astrophys. J. **131**, 375 (2006).
[64] M. G. Walker *et al.*, Astrophys. J. **131**, 2114 (2006).
[65] R. R. Munoz *et al.*, Astrophys. J. **649**, 201 (2006).
[66] M. G. Walker *et al.*, Astrophys. J. **642**, L41 (2006).
[67] S. Mashchenko, A. Sills, and H. M. P. Couchman, Astrophys. J. **640**, 252 (2006).
[68] E. L. Lokas, G. A. Mamon, and F. Prada, Mon. Not. R. Astron. Soc. **363**, 918 (2005).
[69] L. E. Strigari *et al.*, Astrophys. J. **657**, L1 (2007).
[70] L. E. Strigari *et al.*, Astrophys. J. **652**, 306 (2006).
[71] A. A. Klypin, A. V. Kravtsov, O. Valenzuela, and F. Prada, Astrophys. J. **522**, 82 (1999).
[72] B. Moore *et al.*, Astrophys. J. **524**, L19 (1999).
[73] F. Stoehr, S. D. M. White, G. Tormen, and V. Springel, Mon. Not. R. Astron. Soc. **335**, L84 (2002).
[74] S. Ritz (private communication).
[75] P. Sreekumar *et al.* (EGRET), Astrophys. J. **494**, 523 (1998).
[76] S. D. Hunter *et al.*, Astrophys. J. **481**, 205 (1997).